Geothermics 64 (2016) 527–537

Contents lists available at ScienceDirect

Geothermics

journal homepage: www.elsevier.com/locate/geothermics

Three-dimensional geo-electrical structure in Juncalito geothermal prospect, northern Chile

Karin García[a,b,*], Daniel Díaz[a,b]

[a] Departamento de Geofísica, Facultad de Ciencias Físicas y Matemáticas, Universidad de Chile, Blanco Encalada 2002, Santiago, Chile
[b] Centro de Excelencia en Geotermia de los Andes (CEGA), Facultad de Ciencias Físicas y Matemáticas, Universidad de Chile, Plaza Ercilla 803, Santiago, Chile

ARTICLE INFO

Article history:
Received 30 March 2016
Received in revised form 28 July 2016
Accepted 1 August 2016
Available online 11 August 2016

Keywords:
Magnetotelluric method
Central volcanic zone (CVZ)
Geothermal reservoir
Andes

ABSTRACT

Magnetotelluric (MT) data were recorded to investigate a geothermal prospect in northern Chile. The exploration area is located in the Atacama region, at the southern edge of the Chilean Altiplano, at an altitude of ~4100 masl. This area belongs to the southern end of the Central Volcanic Zone (CVZ), a segment of the Andean Volcanic Belt associated with the oblique subduction of the Nazca plate beneath the South American plate. In the surveyed area of 19 MT sites, a two-dimensional geometry and an almost N-S geo-electric strike angle were obtained. A 3-D inversion was carried out and the obtained resistivity model shows a low resistivity layer (<10 Ωm) thicker westward of the profile. This result agrees with the classic pattern of the geo-electric structure in a geothermal system with potential (Anderson et al., 2000; Spichak and Manzella, 2009). The results from these magnetotelluric measurements were compared with different geophysical and geological information gathered in this area, helping to understand the geo-electrical structure obtained by magnetotellurics and to characterize this geothermal prospect. Different possible scenarios, given the available data, are shown.

1. Introduction

The electrical resistivity, obtained by electrical or electromagnetic methods, is particularly useful in geothermal exploration because this parameter has strong variation in these systems. The resistivity is sensitive to temperature, porosity (only if the porosity has interconnected pores and they are filled with fluid), salinity, and clay content. Conceptually a geothermal system consists of a heat source, a transport zone for geothermal fluids, an impermeable cap, and sometimes, a reservoir that stores the heat. The impermeable cap is produced by prolonged fluid circulation reactions on the rock. At temperatures between 70 °C and 200 °C alteration minerals such as smectite and illite form. At higher temperatures, over 220 °C, chlorite-epidote alteration minerals form (Muñoz, 2014). Some clay minerals, such as smectite and illite-smectite are electrically conductive as they have loosely bound cations. On the other hand, chlorite-epidote has all its ions bound in a crystal lattice and, therefore, they are less electrically conductive than illite-smectite minerals (Deer et al., 1962; Pellerin et al., 1996; Anderson et al., 2000; Spichak and Manzella, 2009; Flócvenz et al., 2005; Ussher et al., 2000). Alteration is often unaffected by subsequent cooling, and in most cases, the resistivity structure can be regarded as a "maximum thermometer" (Árnason et al., 2010). In a classic model of a geothermal system, the upflow is a zone in the reservoir where the fluid flow is predominantly vertical, and generally the temperature increases with depth. In upflow areas, the base of the conductive clay cap is often elevated because of the relative increase, with temperature, caused by higher resistivity minerals in the mixed layer (Muñoz, 2014).

The Central Volcanic Zone (CVZ) at the Chilean Andes (Fig. 1) includes 44 active volcanic edifices, as well as more than 18 active minor centers and/or fields, and at least 6 potentially active centers and/or caldera systems (Stern, 2004), located in a highly elevated (>4000 masl) region. In the southern segment of the CVZ (northern Chile) the Nazca plate is being subducted in a direction of 27° (Stern, 2004). The modern volcanic front is located in the western Cordillera Occidental, 120 km above the subducted slab and 240–300 km east of the trench. Crustal thickness reaches ~70 km (Asch et al., 2006) and the basement age ranges from late Precambrian to Paleozoic. The active volcanoes overlie volcanic rocks of Late Oligocene to Quaternary age. Many of these older volcanic centers are extremely well preserved because of the hyper-arid conditions in the region (Stern, 2004). Andesites, dacytes and rhyolites are the dominant rock type.

* Corresponding author at: Centro de Excelencia en Geotermia de los Andes (CEGA), Facultad de Ciencias Físicas y Matemáticas, Universidad de Chile, Plaza Ercilla 803, Santiago, Chile.
E-mail address: kgarcia@ing.uchile.cl (K. García).

http://dx.doi.org/10.1016/j.geothermics.2016.08.001
0375-6505/

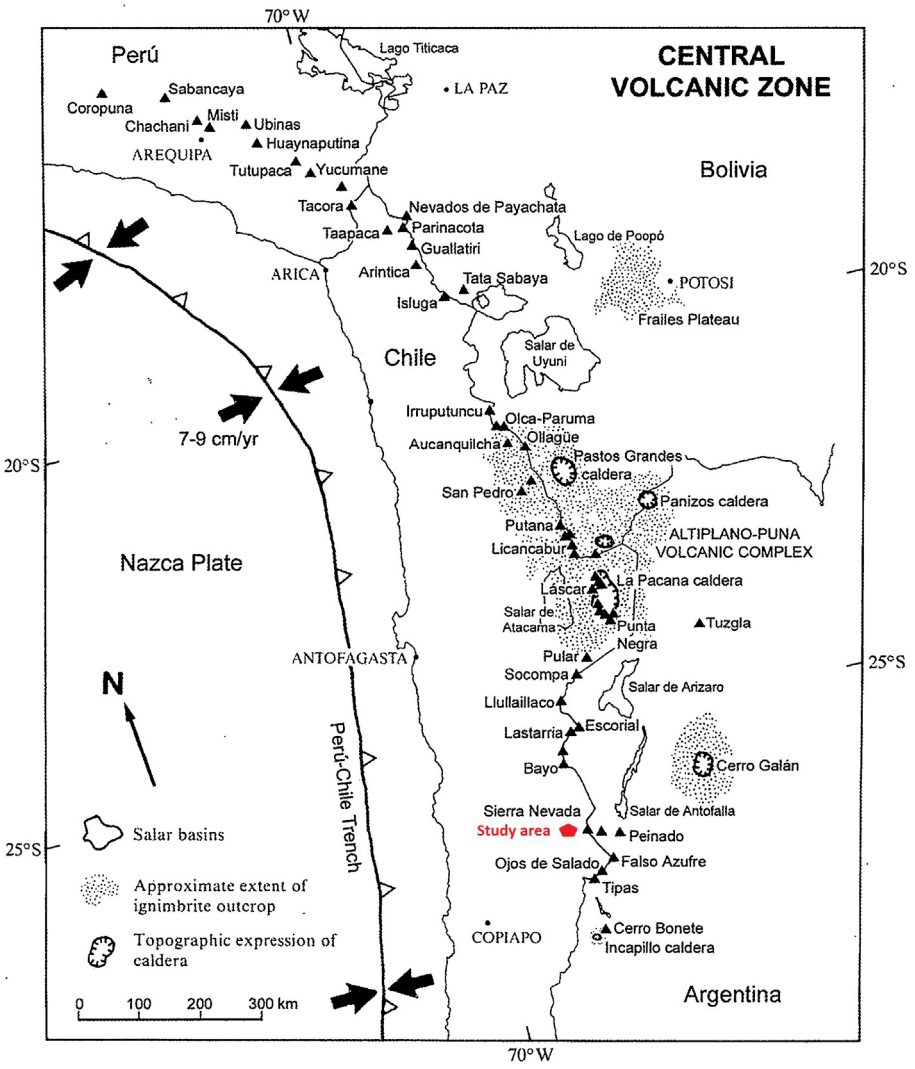

Fig. 1. Regional map of the Central Volcanic Zone (CVZ). Modified from Stern (2004).

In northern Chile (17°S–28°S) during the Pliocene and Quaternary periods, an extensional tectonic phase produced differential block upliftings along N-S trending fault systems. Volcanic vents and hydrothermal manifestations occur associated with small grabens connected with these fault systems (eg. El Tatio and Puchuldiza geothermal fields), on the western side of the Pliocene-Holocene Central Volcanic Zone (Lahsen et al., 2005). In northern Chile there are about 90 hot spring areas, and 45 exploration concessions are being surveyed. The most advanced programs have been carried out in the Colpitas, Apacheta, Pampa Lirima, and El Tatio-La Torta geothermal areas. Meanwhile, exploitation concessions have been granted for the Apacheta and El Tatio La Torta Projects, where production wells have been drilled (Lahsen et al., 2015).

The main target of this research, Juncalito geothermal prospect, is located in the Atacama region, 180 km northeast of Copiapo (see Fig. 2 for details). This area is on the southern side of the CVZ. Even further south, the absence of astenospheric mantle above the flat slab segment precludes the occurrence of arc magmatism (Tassara et al., 2006).

Several indicators such as the closeness to volcanoes and surface expressions of a geothermal field (soil with hydrothermal alteration and high temperature (40.2 °C) hot springs) hint at a high geothermal potential in the Juncalito area (Clavero et al., 1997, 1998). These expressions are weaker than in other high temperature geothermal areas e.g. Hengill geothermal field in Iceland (Gasperikova et al., 2015), Coso geothermal field in USA (Newman et al., 2005) or Taupo volcanic zone in New Zealand (Heise et al., 2008; Bertrand et al., 2015). However there are blind geothermal fields that show no signs of geothermal activity at the surface (Vice et al., 2007; Kratt et al., 2008).

In this work we present the results of 3-D resistivity modeling obtained with magnetotelluric data (MT) and a comparison with different geophysical and geological information gathered in this area, which is used to understand the geo-electrical structure obtained from magnetotellurics and to assess the geothermal potential of Juncalito prospect.

2. Geological setting

The MT data was collected at Llano los Cuyanos, a flat area at approx. 4100 masl., surrounded by alluvial deposits of Pliocene age to the NW, and alluvial-colluvial deposits of Pleistocene to Holocene age to the SE. In the northeast end of the area, the Azufrera los Cuyanos volcano is located. It belongs to a recent volcanic and stratovolcanic complex (Pleistocene to Holocene). On the slope of this volcano, hydrothermal alteration is observed. On the southeastern side of this area there is an older volcanic and stratovolcanic

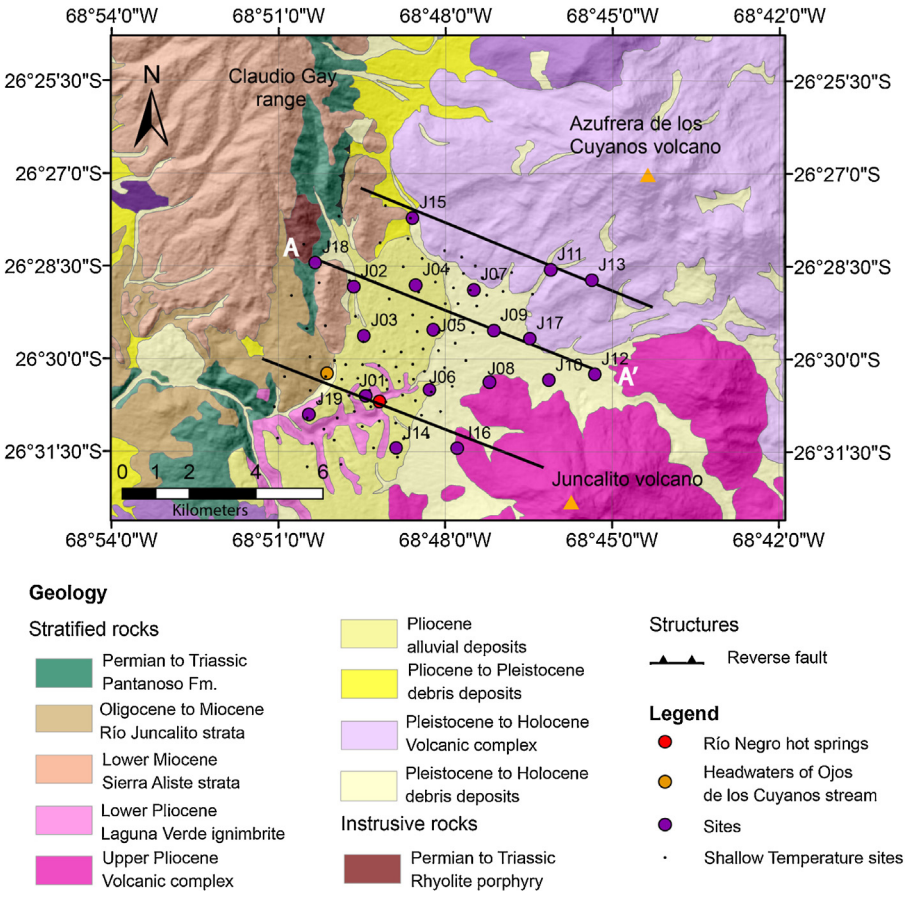

Fig. 2. Geological setting with MT sites. Modified from Clavero et al. (1997, 1998).

complex of Pliocene age. On the southwestern slope of this volcano, hydrothermal alteration is observed. On the western edge of the study area, the Claudio Gay mountain range is located. Hot water springs at 40.2 °C (Risacher et al., 2011) can be found at the southern edge of the study zone (Río Negro springs, see Fig 2). Cation geothermometers measured in Río Negro springs suggest temperatures in the range between 101 °C and 223 °C but this geothermometry is of low confidence because of the dilution-mixing process of alteration waters with brines from the salars. However, a positive compositional indicator of the Río Negro springs is the silica concentration (130–160 mg/kg SiO_2) indicating quartz equilibration temperatures of 140–160 °C (Lira et al., 2012 and references therein).

According to the geology of Llano los Cuyanos area (Clavero et al., 1997, 1998), we can distinguish between basement and cover, as described below. The cover consists of volcanic and unconsolidated deposits. The volcanic deposits consist of Laguna Verde ignimbrite, and below this, it is possible to find units of Permian to Miocene age, consisting of sedimentary and volcanoclastic deposits.

In the study area, other geological and geophysical studies were performed, helping to describe the Juncalito geothermal prospect. In particular, we discuss soil CO_2 surveys, surface temperature, and gravimetry. All these studies will be discussed more thoroughly in the Complementary Methods section.

3. Magnetotelluric data

The magnetotelluric method (MT) linearly relates the horizontal electric and magnetic fields to the impedance tensor (also known as the transfer function) in the frequency domain. The impedance tensor contains information about the resistivity structure. Similarly, the geomagnetic transfer function (or tipper) is also linearly related to the vertical and horizontal components of the magnetic field, indicating lateral resistivity contrasts when plotted as induction arrows. Furthermore the phase tensor, which is a function of the impedance tensor, was used. Phase tensor parameter is very useful because, in contrast to the impedance tensor, it is independent of distortion caused by near surface heterogeneities (see more details in Caldwell et al. (2004)). The phase tensor can be represented graphically as ellipses, providing information about the dimensionality of the geo-electrical structure. Resistivity gradients are shown by the magnitude of the phase response, the invariant ϕ_2 (geometric mean of the principal values ϕ_{max} and ϕ_{min} of the phase tensor – $\phi_2 = \sqrt{(\phi_{\max}\phi_{\min})}$). The period is related closely to the depth, with short periods corresponding roughly to shallow depths while long periods correspond to greater depths. For example, if the phase tensor invariant parameter ϕ_2 is larger than 45° at short periods, it implies that the electrical conductivity at shallow depths beneath the station is relatively high (with respect to the same station at different periods).

The time series for electric and magnetic fields measured in the study area were processed using robust processing techniques based on Egbert and Booker (1986) in order to obtain the impedance tensor and the geomagnetic transfer functions.

Data was collected using the ADU07 equipment from Metronix. 19 MT sites (Fig. 2) were obtained in May 2012. Spacing between measurement sites is between 1 and 2 km.

At each site, the horizontal components of both the electric and magnetic fields and the vertical component of the magnetic field were measured in order to obtain the transfer function and the geomagnetic transfer function.

3.1. Dimensionality of the geo-electric structure

3.1.1. Phase tensor

Dimensionality of the geo-electric structure was studied before making the appropriate inversion (1-D, 2-D, 3-D). Fig. 3 shows phase tensor ellipses, at different periods, to determine the dimensionality and orientation of the geo-electric structure, as well as the resistivity gradients.

Top left plot at Fig. 3 shows the phase tensor at 31 ms (shallow depth). The phase tensor tends to be a circle, indicating that the shallower part of the structure is 1-D. Additionally, these circles are red ($\phi_2 > 45^\circ$), indicating that the structure is conductive at a shallow depth. At 695 ms, (top right plot, deeper than 31 ms plot) the darker red color is only seen in the west, indicating that the conductive structure reaches greater depth in the western part of the survey area. A transition to a more resistive body begins eastwards. At 8 s (bottom left plot), the ellipses are oriented almost NS, indicating that the structure is 2-D at this period. Their blue tones ($\phi_2 < 45^\circ$) indicate increasing resistivity below the conductive surface layer. At 256 s, ellipses remain aligned and ϕ_2 increases again with a slight tendency to increase in conductivity at a greater depth.

3.1.2. Geo-electrical strike

The method described in Smith (1995) was used to obtain the angle of the geo-electric strike, which considers telluric distortion occurring in structures near the surface that are not one-dimensional. Using distortion matrices, the distorted electric field is written as a function of the values the electric field would have if the inhomogeneities were not present.

Fig. 4 shows a clear trend of a geo-electric strike, indicating that the best geo-electrical strike is N10°E or N100°E. The result shows an ambiguity of ±90° that can be solved using induction arrows, which are shown in the following section. A 2-D inversion along a profile perpendicular to the geo-electrical strike would be suitable for most of the dataset, and was carried out along profile A-A′ (see Fig. 2 for location of profile). However, as the resistivity structure at depths of interest is likely to be three-dimensional (top left plot in Fig. 3), 3-D inversions were performed, showing a good agreement with the 2-D inverted model.

3.1.3. Induction arrows

Fig. 3 shows four plots of induction arrows at different periods. Top left plot is at 31 ms and shows arrows of very small magnitude,

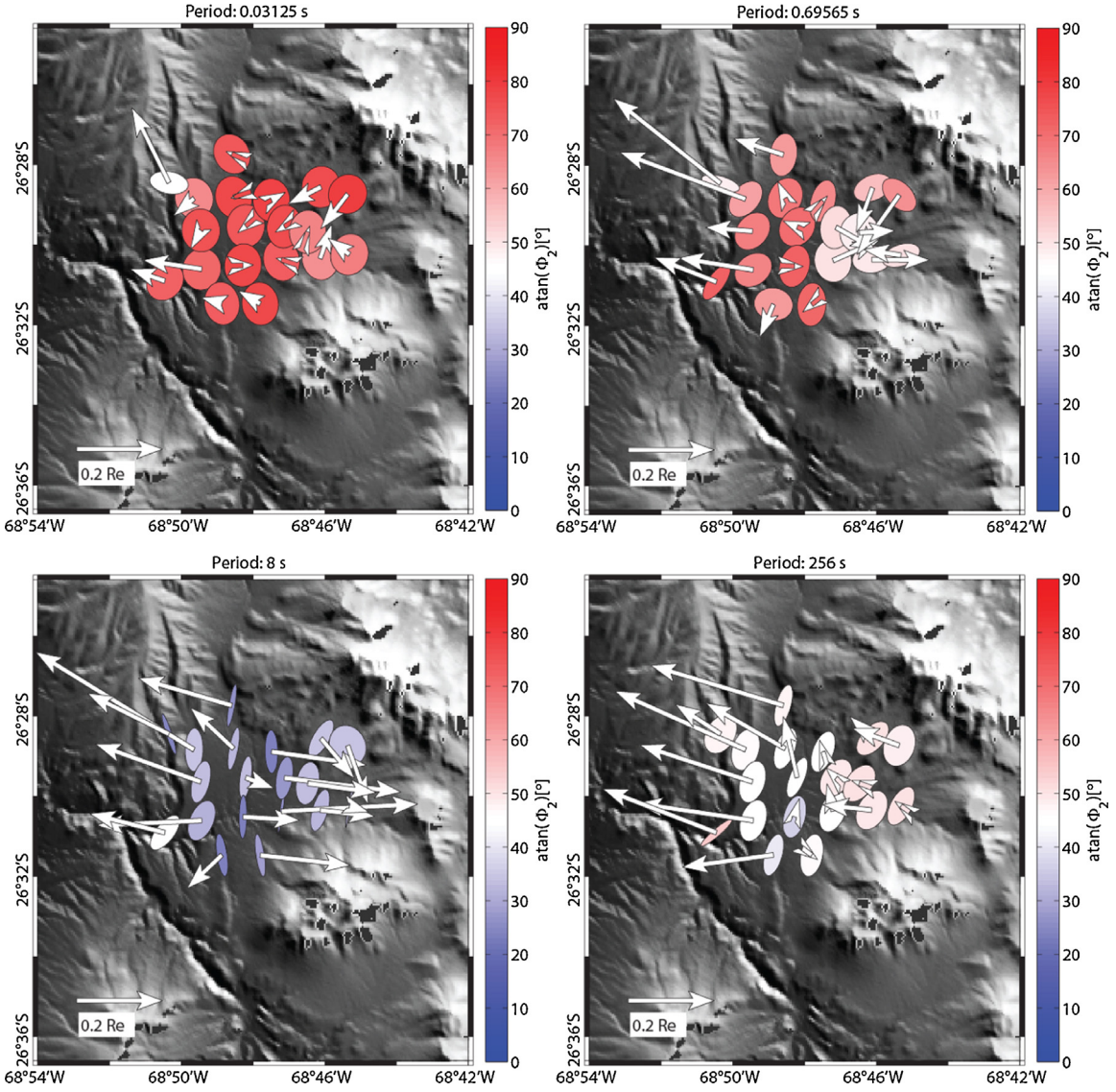

Fig. 3. Phase tensor and induction arrows (real part of geomagnetic transfer function according to Wiese convention, i.e., arrows point outward from a conductor) plotted at different periods between 0.01 and 1000 s.

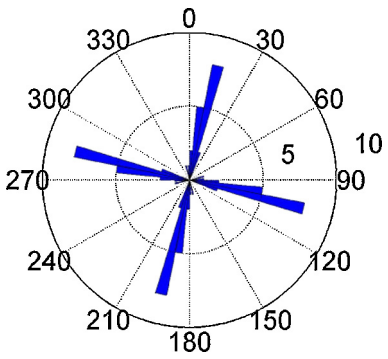

Fig. 4. Rose diagram showing the strike angle for all sites and periods between 1 and 10 s. The best geo-electrical strike is N10°E or N100°E.

indicating that the horizontal resistivity contrast is minor. This suggest that, at this period, the structure is almost one-dimensional. At a period of 8 s, the arrows are longer and point away from a main axis oriented NNE-SSW (i.e. there is no more ambiguity in the estimated geo-electric strike calculated in the previous section and the strike value is N10°E), consistently with the occurrence of a geothermal domain. For larger periods, the induction arrows point towards the northwest, i.e., away from the volcano. This could be related to a large conductive structure at depths of several kilometers, just below the volcanic edifices in this area.

3.2. 3-D inversion

We carry out a 3-D instead of a 2-D inversion, as the resistivity structure at depths of interest is likely to be three-dimensional (top right plot in Fig. 3) as we will see in this section.

Using data from 19 stations measured in the study area, a 3-D model was obtained using the ModEM code described by Egbert and Kelbert (2012) and Kelbert et al. (2014). The inversion procedure is based on Non-Linear Conjugate Gradients (NLCG) and the program is parallelized (using MPI) in order to work on various processors at the same time. For the 3-D case, all the elements of the impedance tensor are significant, and therefore, this method considers the inversion of its four components, plus two elements of the geomagnetic transfer function, setting an error floor of 10% for the components inverted. Data at 6 periods per decade were used in a period range of 0.002 s and 512 s. The study area was discretized with a grid of 200 m × 200 m in horizontal directions at the central part of the model, where all the measured stations are placed, and increased while moving away from the central part. Various inversions were performed in order to obtain the smoothest model which could fit the data properly. Three slices on the final model resulting from 3-D inversion are shown in Fig. 5, obtaining a normalized RMS error of 1.8. For examples of the data fit, see Fig. A.8 in the supporting information.

Fig. 5 shows three resistivity profiles (see Fig. 2 for location of profiles) obtained from the 3-D modeling. These profiles are approximately orthogonal to the geo-electrical strike and have an

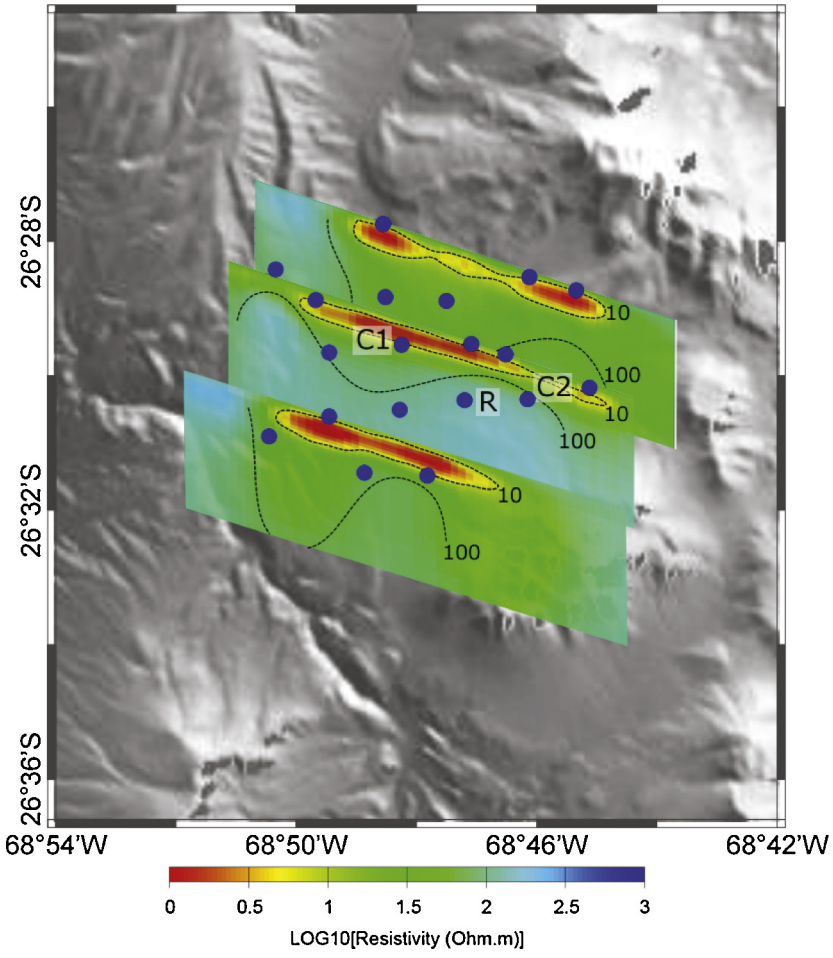

Fig. 5. Three slices of the 3-D model obtained from the inversion process. All slices have a depth extension of 4 km, and an approximate horizontal extension of 10 km. Blue circles indicate location of measured stations. Segmented lines indicate 10 and 100 Ωm values. Structures marked as C1, C2 and R are discussed in the main text. (For interpretation of the references to color in this figure legend, the reader is referred to the web version of this article.)

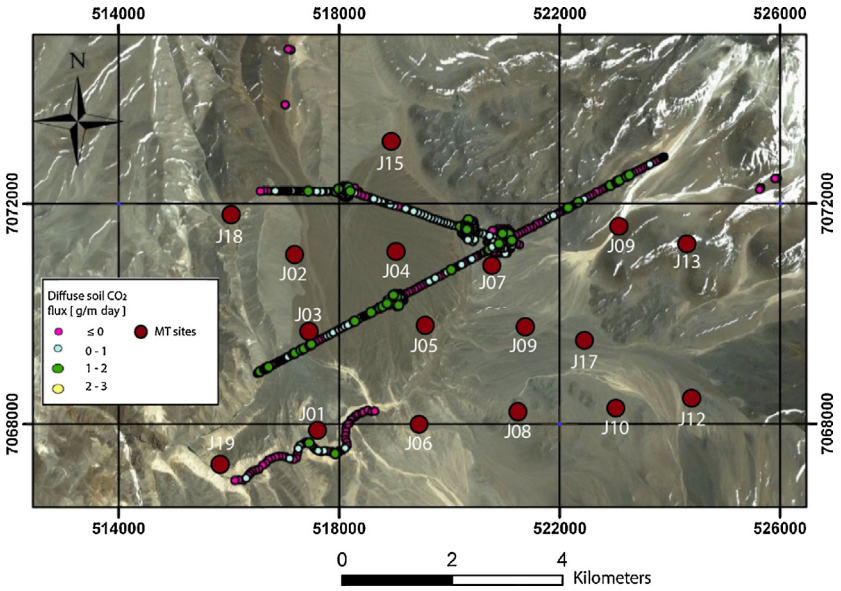

Fig. 6. Diffuse soil CO_2 flux in units of [g/m^2-day]. Modified from Navarrete (2012).

orientation of N100°E. The main geo-electric structures are a resistive cover, a conductive layer (C1 and C2) which becomes thicker at the west (C1) of the profile, and an oval resistive body (R) below the conductive layer at the east of the profile. It is possible to identify conductive structures (C1 and C2). These features are thicker at the western half of the profile, which is consistent with the results of the phase tensor (see Fig. 3 in 695 ms plot), as the phase tensor ellipses are also indicating a deeper conductive zone to the west of this area. If one follows the classical resistivity structure of a geothermal system, according to Anderson et al. (2000) and Spichak and Manzella (2009), C2 could represent a thinner clay cap with an elevated base in this part of the study area indicating possible higher temperature alteration at shallower depth.

4. Complementary methods

Other studies in geology and geophysics were performed in the study area, which helped with the description of the Juncalito geothermal prospect and which are discussed below.

4.1. Diffuse soil CO_2

Navarrete (2012) studied the diffuse soil CO_2 flux (see Fig. 6), because CO_2 is usually one of the most abundant gases in geothermal systems associated with volcanism. In Juncalito, the CO_2 flow values measured were very low (see Fig. 6). This means that there isn't much gas in the ascending geothermal fluid or that there is some mechanism that prevents its ascent, which may be associated with an impermeable cover (a seal cap), such as clay-rich volcanic deposits (Laguna Verde ignimbrite). Over this cover there can be found recent volcanic deposits of Juncalito and Azufrera de los Cuyanos volcanoes which, taken together, may be sufficiently impermeable to restrict gas upflow.

4.2. Surface temperature

Lira et al. (2012) performed a study of surface temperature in Llano los Cuyanos. The study obtained thermal anomalies associated with springs and also with areas without hydrothermal discharge. Lira et al. (2012) recognized two areas of thermal anomalies with hydrothermal discharge: (1) Headwaters of Ojos de los Cuyanos stream: found to the west of the measurements (see Fig. 2), with anomalous temperatures greater than 15 °C (background temperature <9 °C, during the study period), and aligned NS. (2) To the south: Río Negro springs (see Fig. 2) with an anomalous temperature >30°C, and aligned NE-SW. Additionally, a third anomaly – at about 11 °C and without surface water expression like the others – is located on the west slope of Azufrera de los Cuyanos volcano. This anomaly could be related to a fault-controlled circulation of meteoric waters or to a thermal aquifer that discharge into the Río Negro springs, with a deeper heat source associated with Azufrera de los Cuyanos and Juncalito volcanoes.

Finally, considering the results of the resistivity structure of the geothermal prospect, it can be suggested that the upflow (ascending flow from the heat source) of the geothermal system could be in the SW flank of the Azufrera de los Cuyanos volcanic complex. The outflow (cooled flow discharge) could take place in Río Negro springs and in headwaters of Ojos de los Cuyanos stream (Lira et al., 2012).

4.3. Gravimetry

In Lira (2013) gravimetry measurements and results are described. Lira (2013) performed a gravimetric study and obtained a residual gravity anomaly map (background density: 2.6 g/cc. See Fig. 7). On the west side of the MT sites the residual anomaly is more negative than on the east side. This means that the western layer is of lower density and/or thicker than the eastern one.

The layers associated with low density can be related to rock with high porosity. In this context and compared with the MT method, an area with layers with high porosity, and where fluids circulation occurs, would give as a result a low resistivity anomaly. This implies that, in this case, low density and/or thicker layers are to be found to the west side of the measurements, and also according to the MT method, a low resistivity anomaly can be observed, being thicker to the west than to the east of the sites. Thus, the results obtained with the gravimetric method support the MT results.

5. Discussion

Different scenarios, that could be described using the available data, are discussed.

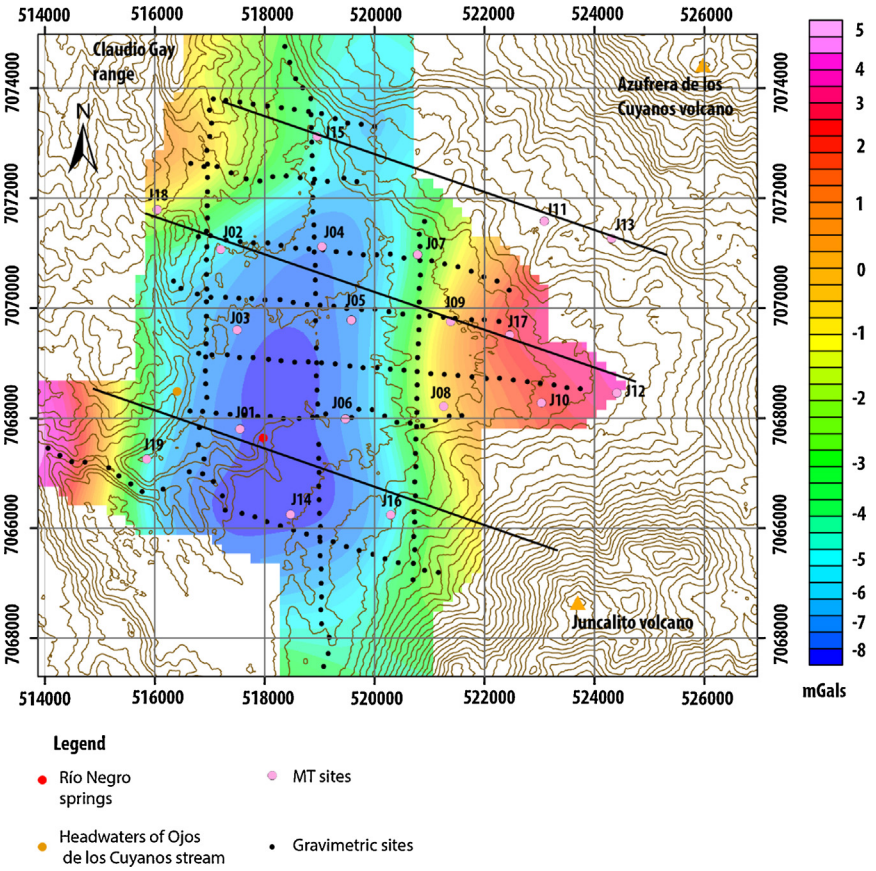

Fig. 7. Residual gravity anomaly map. Background (2600 kg/m^3). The pink circles represent the MT sites, black circles are the gravimetric sites and lines are location of MT profiles shown in Fig. 5. (For interpretation of the references to color in this figure legend, the reader is referred to the web version of this article.)

A possible scenario is that Juncalito prospect is not a geothermal resource and the studied methods indicate that:

1. There is not diffuse CO_2 ascending.
2. The surface temperature anomaly could be related to a fault-controlled circulation of meteoric water.
3. Considering the gravity measurements, R could also be related to a denser body of a crystalline kind, which would also correspond to the relatively high resistivity values.
4. The conductive anomaly (C1 and C2) would be originated by ancient evaporitic sequences. And/or the conductive layer may still be a hot outflow from a distant source that could be outside the measured area

On the other hand, there is evidence for Juncalito being a geothermal resource if we consider the results from:

1. The silica geothermometer, suggesting high temperatures of >140 °C.
2. Some mechanism that prevents the ascent of diffuse soil CO_2, which may be associated with an impermeable cover.
3. The surface temperature anomaly that is caused by a deep source associated with the Azufrera de los Cuyanos and Juncalito volcanoes.
4. The resistivity structure obtained from the MT method, according which:
   (a) The conductivity layer (C1 and C2) may be the response from clay minerals originated by hydrothermal alteration.
   (b) The resistive body R, situated under the updomed base in the C2 conductor, could be a reservoir.

With all these data collected in the Juncalito area, this prospect could be defined as an inferred resource (the thermal energy may be estimated with a low level of confidence).

6. Conclusions

The geothermal exploration in northern Chile, in particular in Juncalito prospect, is difficult because of the possible presence of evaporitic sequences that misrepresent the signal obtained from different geological and geophysics methods. For instance, the results obtained with the cation geothermometers are not reliable (Gigenbach, 1988) and it is necessary to use other methodologies. On the other hand, the electrical resistivity signal of a geothermal system may blend together with the signal of electrical response from the evaporitic sequences. Therefore it is required to gather together as much geological and geophysical data as possible to understand the studied system. However, to get a better level of confidence concerning the resource, it is essential to drill and make direct reservoir measurements from well data.

Acknowledgements

We would like to thank EASA for their logistic support and permission to carry out this work, in particular to Aldo Giavelli, and the

geological and geophysical service companies: Geovectra, Zonge and TRV that partially founded this work. Moreover, this research was supported by the Andean Geothermal Center of Excellence (CEGA), FONDAP project 15090013. We would also like to thank Arturo Belmonte, Anne Schlachli, and Fernando Zamudio for their fieldwork assistance, as well as Gonzalo Yañez and Diego Morata for their suggestions and proofreading. We would like to thank A. Kelbert, G. Egbert and N. Meqbel, for provide acces to ModEM inversion routines, and N. Meqbel for provide a model and data visualizer, 3D-Grid.

Appendix A. Data fits

The following figures represent the data fit as a comparison between measured (circles for apparent resistivity and phase, for both off-diagonal elements of the impedance tensor), and modeled data (filled circles for apparent resistivity and phase), for the 19 measured sites. The modeled data was obtained using ModEM software trying to fit the full impedance tensor and tipper data for each site. Error bars of the measured data are smaller than symbol size in most cases.

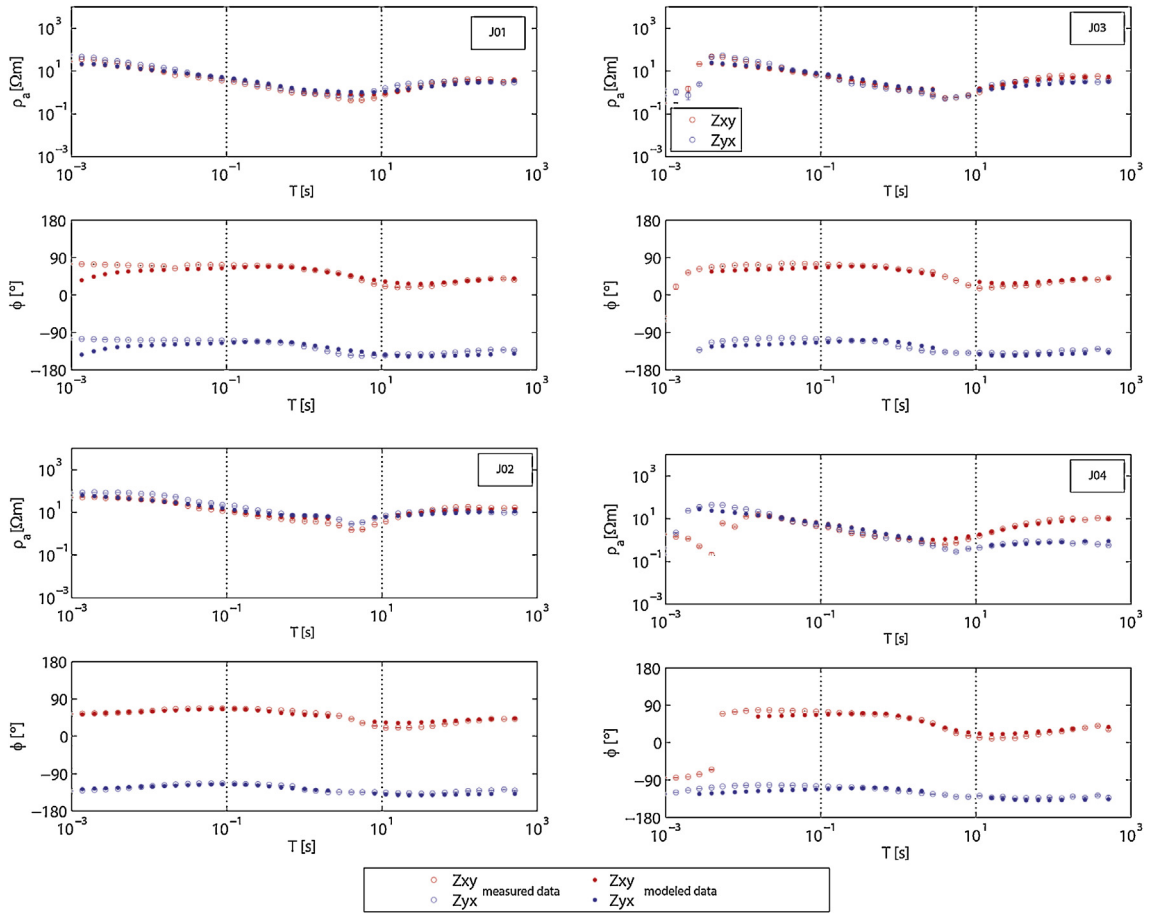

Fig. A.8. Data fit as a comparison between measured (circles for apparent resistivity and phase, for both off-diagonal elements of the impedance tensor), and modeled data (filled circles for apparent resistivity and phase), for the 19 measured sites.

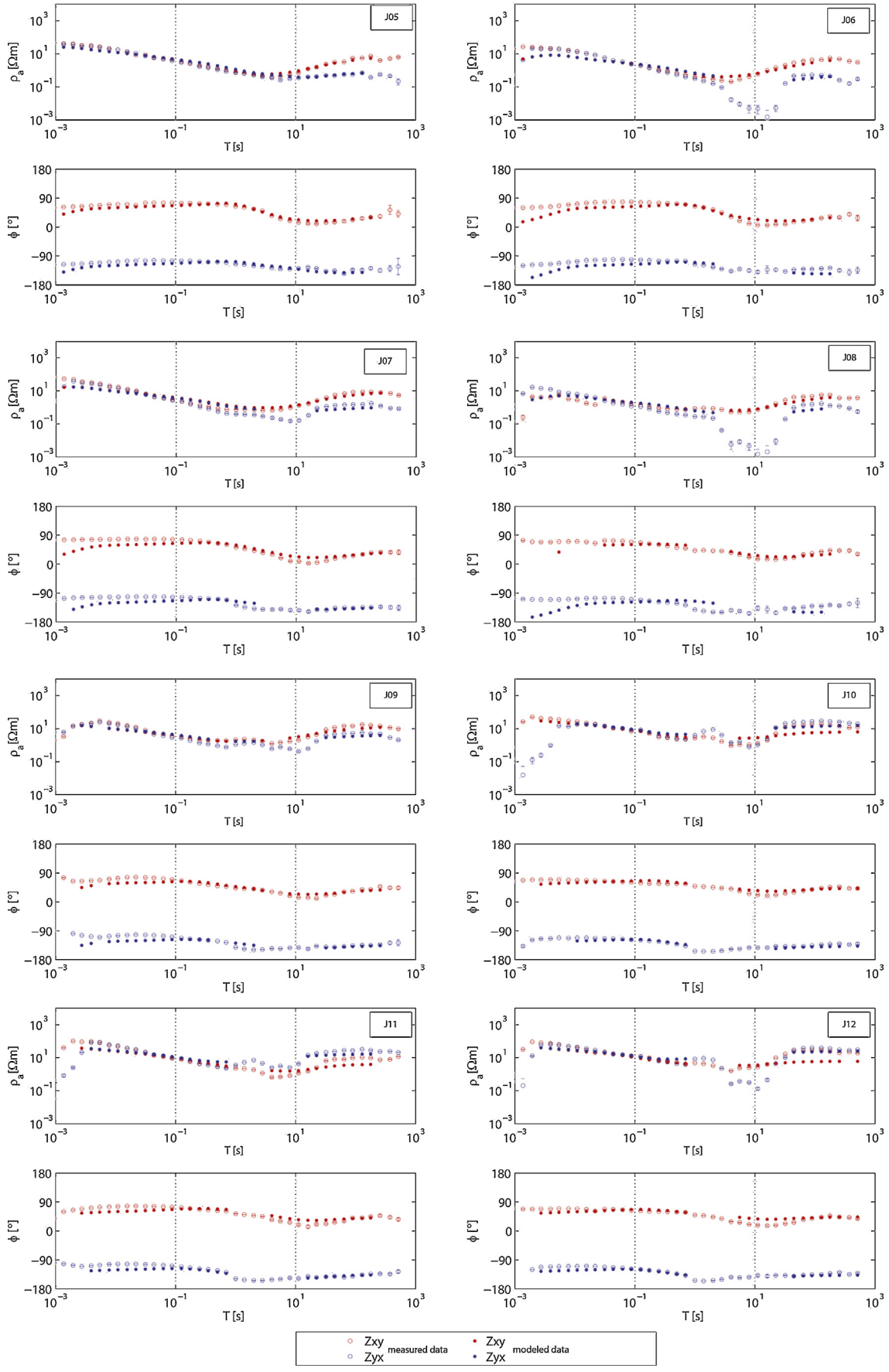

Fig. A.8. (*Continued*)

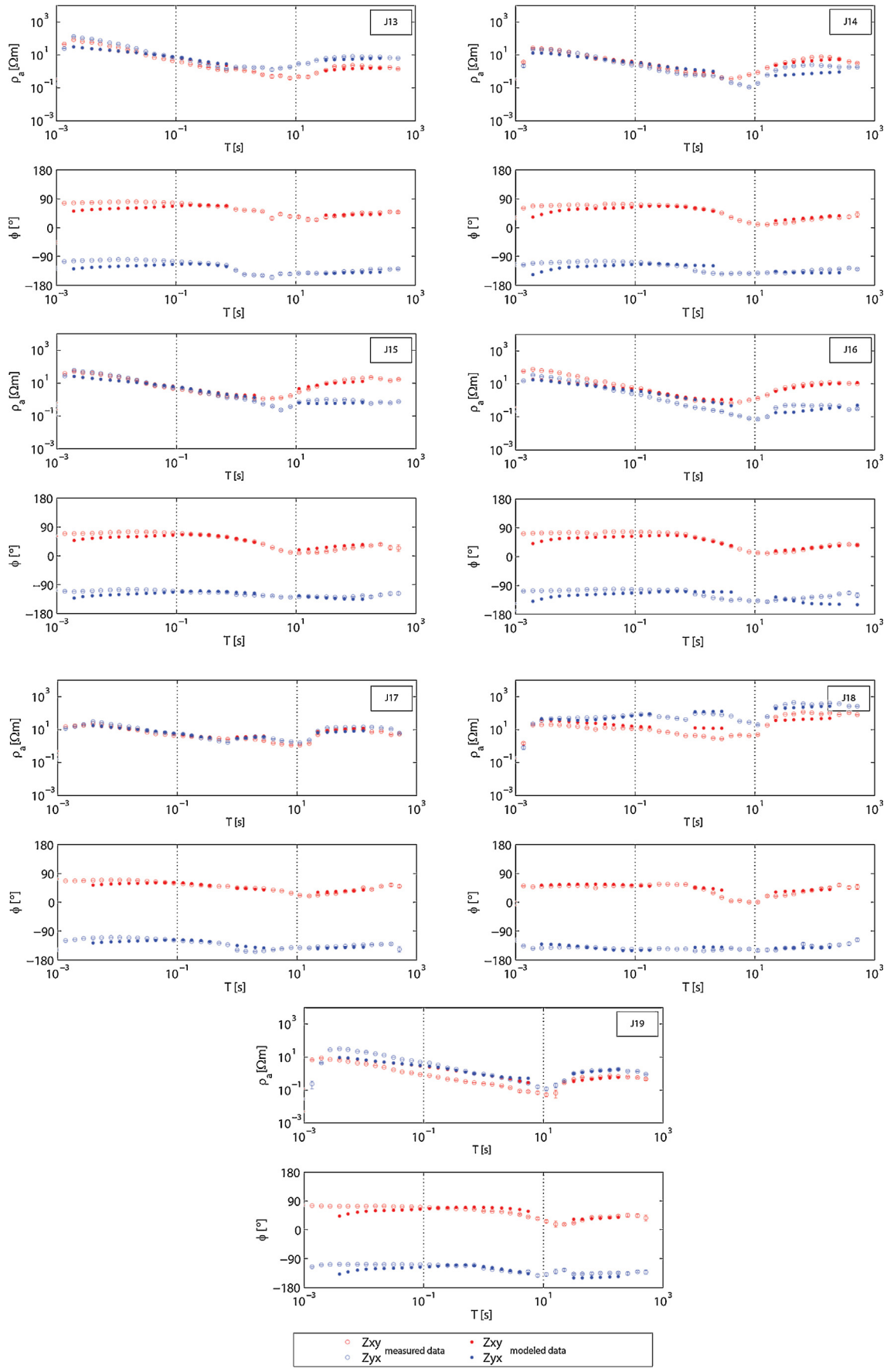

Fig. A.8. (*Continued*)

References

Árnason, K., Eysteinsson, H., Hersir, G.P., 2010. Joint 1D inversion of {TEM} and {MT} data and 3D inversion of {MT} data in the hengill area, {SW} Iceland. Geothermics 39 (1), 13–34, http://dx.doi.org/10.1016/j.geothermics.2010.01.002, the European I-GET Project: Integrated Geophysical Exploration Technologies for Deep Geothermal Reservoirs. http://www.sciencedirect.com/science/article/pii/S0375650510000039.

Anderson, E., Crosby, D., Ussher, G., 2000. Bulls-eye!-simple resistivity imaging to reliably locate the geothermal reservoir. In: Proceedings of the 2000 World Geothermal Congress, May, Kyushu-Tohoku, Japan, pp. 909–914.

Asch, G., Schurr, B., Bohm, M., Yuan, X., Haberland, C., Heit, B., Kind, R., Woelbern, I., Bataille, K., Comte, D., Pardo, M., Viramonte, J., Rietbrock, A., Giese, P., 2006. Seismological studies of the central and southern Andes. In: Oncken, O., Chong, G., Franz, G., Giese, P., Gtze, H.-J., Ramos, V., Strecker, M., Wigger, P. (Eds.), The Andes, Frontiers in Earth Sciences. Springer Berlin Heidelberg, pp. 443–457, http://dx.doi.org/10.1007/978-3-540-48684-8_21.

Bertrand, C.T.G., Bannister, E.A.,S., Soengkono, S., Bennie, S.L., Hill, G.J., Heise, W., 2015. Using array MT data to image the crustal resistivity structure of the southeastern Taupo volcanic zone, new zealand. J. Volcanol. Geother. Res. 305, 63–75, http://dx.doi.org/10.1016/j.jvolgeores.2015.09.020.

Caldwell, T.G., Bibby, H.M., Brown, C., 2004. The magnetotelluric phase tensor. Geophys. J. Int. 158 (2), 457–469, http://dx.doi.org/10.1111/j.1365-246X.2004.02281.x, arXiv:http://gji.oxfordjournals.org/content/158/2/457.full.pdf+html, http://gji.oxfordjournals.org/content/158/2/457.abstract.

Clavero, J., Mpodozis, O., Gardeweg, M., 1997. Mapa Geológico del Área del Salar de Wheelwright, Región de Atacama. (Servicio Nacional de Geología y Minería Chile), Escala 1-100000.

Clavero, J., Gardeweg, M., Mpodozis, O., 1998. Mapa Geológico del Área del Salar de Piedra Parada, Región de Atacama. (Servicio Nacional de Geología y Minería Chile), Escala 1-100000.

Deer, W., Howie, R., Zussman, J., 1962. Sheet silicates. In: Rock-forming Minerals, pp. 443–457.

Egbert, G.D., Booker, J.R., 1986. Robust estimation of geomagnetic transfer functions. Geophys. J. Int. 87 (1), 173–194, http://dx.doi.org/10.1111/j.1365-246X.1986.tb04552.x, arXiv:http://gji.oxfordjournals.org/content/87/1/173.full.pdf+html, http://gji.oxfordjournals.org/content/87/1/173.abstract.

Egbert, G.D., Kelbert, A., 2012. Computational recipes for electromagnetic inverse problems. Geophys. J. Int. 189 (1), 251–267, http://dx.doi.org/10.1111/j.1365-246X.2011.05347.x.

Flócvenz, Ó.G., Spangenberg, E., Kulenkampff, J., Árnason, K., Karlsdóttir, Ragna, Huegens, E., 2005. The role of electrical interface conduction in geothermal exploration. In: Proceedings of the World Geothermal Congress 2005, Antalaya, Turkey, pp. 24–25.

Gasperikova, E., Rosenkær, G.K., Arnason, K., Newman, G.A., 2015. Resistivity characterization of the Krafla and Hengill geothermal fields through 3D MT inverse modeling. Geothermics 57, 246–257.

Gigenbach, W., 1988. Geothermal solute equilibria. derivation of na-k-mg-ca geoindicators. Geochim. Cosmochim. 52, 2749–2765.

Heise, W., Caldwell, T.G., Bibby, H.M., Bannister, S., 2008. 3-D modelling of magnetotelluric data from the Rotokawa geothermal field, Taupo volcanic zone, New Zealand. Geophysics 173, 740–750.

Kelbert, A., Meqbel, N., Egbert, G.D., Tandon, K., 2014. Modem: a modular system for inversion of electromagnetic geophysical data. Comput. Geosci. 66, 40–53, http://dx.doi.org/10.1016/j.cageo.2014.01.010.

Kratt, C., Coolbaugh, M., Sladek, C., Zehner, R., Penfield, R., Delwiche, B., 2008. A new gold pan for the west: discovering blind geothermal systems with shallow temperature surveys. In: Geothermal Resources Council.

Lahsen, A., Sepulveda, F., Rojas, J., Palacios, C., 2005. Present status of geothermal exploration in Chile. In: Proceedings of the World Geothermal Congress 2005, Antalaya, Turkey.

Lahsen, A., Rojas, J., Morata, D., Aravena, D., 2015. Geothermal exploration in Chile: country update. In: Proceedings World Geothermal Congress 2015, Melbourne, Australia.

Lira, E., Arcos, R., Clavero, J., Giavelli, A., Mayorga, C., 2012 August. Shallow temperature measurements at Juncalito, a geothermal prospect, Central Andes, Chile. In: Congreso Geológico Chileno 13, Antofagasta, Chile, pp. 618–620.

Lira, E., 2013. Estudio de gravimetría terrestre – Juncalito, Energía Andina internal report.

Muñoz, G., 2014. Exploring for geothermal resources with electromagnetic methods. Surv. Geophys. 35, 101–122, http://dx.doi.org/10.1007/s10712-013-9236-0.

Navarrete, Á., 2012. Origen y comportamiento del CO_2 difuso del suelo en los sistemas geotérmicos de Juncalito (68°55′–68°38′20″ W y 26°25′–26°31′30″ S, Región de Atacama) y Colpitas (69°29′30″–69°23′30″ W y 17°50′30″ S–18°S, región de Arica y Parinacota), Chile, Bachelor thesis. Departamento de Geología, Universidad de Chile, 132 pp. http://www.tesis.uchile.cl/handle/2250/112064.

Newman, G.A., Hoversten, M.G., Wannamaker, P.E., Gasperikova, E.,2005. Magnetotelluric characterization of the COSO geothermal field. In: Workshop on Geothermal Reservoir Engineering. Stanford University, Stanford, CA.

Pellerin, L., Jhonston, J.M., Hohmann, G.W., 1996. A numerical evaluation of electromagnetic methods in geothermal exploration. Geophysics 61, 121–130.

Risacher, F., Fritz, B., Hauser, A., 2011. Origin of components in Chilean thermal waters. J. South Am. Earth Sci. 31 (1), 153–170, http://dx.doi.org/10.1016/j.jsames.2010.07.002.

Smith, J.T., 1995. Understanding telluric distortion matrices. Geophys. J. Int. 122 (1), 219–226, http://dx.doi.org/10.1111/j.1365-246X.1995.tb03549.x, arXiv:http://gji.oxfordjournals.org/content/122/1/219.full.pdf+html, http://gji.oxfordjournals.org/content/122/1/219.abstract.

Spichak, V., Manzella, A., 2009. Electromagnetic sounding of geothermal zones. J. Appl. Geophys. 68 (4), 459–478, http://dx.doi.org/10.1016/j.jappgeo.2008.05.007 http://www.sciencedirect.com/science/article/pii/S0926985108000694.

Stern, C.R., 2004. Active Andean volcanism: its geologic and tectonic setting. Revista geológica de Chile 31, 161–206 http://www.scielo.cl/scielo.php?script=sci_arttext&pid=S0716-02082004000200001&nrm=iso.

Tassara, A., Gtze, H.-J., Schmidt, S., Hackney, R., 2006. Three-dimensional density model of the Nazca plate and the Andean continental margin. J. Geophys. Res.: Solid Earth 111 (B9), b09404, http://dx.doi.org/10.1029/2005JB003976.

Ussher, G., Harvey, C., Johnstone, R., Anderson, E., 2000. Understanding the resistivities observed in geothermal systems. In: Proceedings World Geothermal Congress, pp. 1915–1920.

Vice, G.S., F.J.E., Ehni, W.J., Coolbaugh, M.F., 2007. Structural controls of a blind geothermal system in the northern pyramid lake area, northwestern Nevada. In: Geothermal Resources Council.